Rev.Adv.Mater.Sci. 7 (2004) 41-49

# AN EXAMINATION OF MICROTEXTURE AND MICROSTRUCTURE IN ULTRAFINE-GRAINED NICKEL

**A. P. Zhilyaev [1], M. D. Baró [2], T. G. Langdon [3,4] and T. R. McNelley[1]**

[1] Department of Mechanical Engineering, Naval Postgraduate School, Monterey, CA 93943-5146, USA
[2] Universitat Autònoma de Barcelona, 08193 Bellaterra, Spain
[3] Departments of Aerospace & Mechanical Engineering and Materials Science, University of Southern California, Los Angeles, CA 90089-1453, USA
[4] Also affiliated with Materials Research Group, School of Engineering Sciences, University of Southampton, Southampton SO17 1BJ, U.K.

*Received: May 15, 2004*

**Abstract.** A detailed orientation imaging microscopy (OIM) investigation was conducted to evaluate the microstructural characteristics in samples of pure nickel processed using three different procedures of severe plastic deformation (SPD): equal-channel angular pressing (ECAP), high-pressure torsion (HPT) and a combination of ECAP and HPT. Electron backscattering diffraction (EBSD) techniques were employed to measure the microtextures and the distributions of the misorientation angles. A thorough analysis of the microtexture revealed the shear plane normal and shear direction for UFG nickel obtained by various kinds of severe plastic deformation. It is shown that a combination of ECAP and HPT leads both to a greater refinement in the microstructure and to a smaller fraction of boundaries having low angles of misorientation.

## 1. INTRODUCTION

Recently, much attention has been given to ultrafine-grained (UFG) materials, with grain sizes in the submicrometer or nanometer range, which are expected to have higher strength and toughness than their coarse-grained counterparts [1]. A possibility for attaining a UFG structure is through the use of a processing technique involving the application of severe plastic deformation (SPD): examples of SPD processing include equal-channel angular pressing (ECAP) [2-4], high-pressure torsion (HPT) [3-6], accumulative roll-bonding (ARB) [7-9], friction stir processing (FSP) [10-12] or combinations of these techniques such as ARB followed by FSP [13] or ECAP followed by HPT [14-16]. An important advantage of SPD processing is that the same procedure may be used to introduce UFG structures into a wide range of metallic alloys.

There are two important characteristics defining the UFG structure in metals. First, it is necessary to measure the mean grain size, the distribution of grain sizes, the distribution of the grain boundary misorientations and the texture of the as-processed material. Second, it is important also to examine the thermostability of the UFG microstructure since, if the ultrafine grains are reasonably stable at elevated temperatures, there is a potential for achieving superplastic ductilities at both unusually low testing temperatures and exceptionally rapid strain rates [17]. Despite the fact that an increase in strength is generally associated with a loss in ductility in testing at ambient and low temperatures, recent experiments demonstrated that SPD processing, when taken to a sufficiently high strain, is capable of producing materials exhibiting extraordinary combinations of both high strength and high ductility [1]. This result was attributed to the unique characteris-

Corresponding author: A.P. Zhilyaev, e-mail: AlexZ@anrb.ru

tics of the UFG microstructure produced by SPD processing including the presence of an exceptionally high fraction of non-equilibrium grain boundaries [4].

The two procedures of ECAP and HPT appear to be the most attractive for developing microstructures having reasonably homogeneous distributions of ultrafine and equiaxed grains. In ECAP a bar or rod is pressed through a die constrained within a channel bent into an L-shaped configuration [2,18-20], whereas in HPT a thin disk is subjected to a high pressure and concurrent torsional straining [5,6,21]. Although there have been extensive reports documenting the microstructural evolution taking place during SPD processing in ECAP [22,23] and HPT [6] and the subsequent stability of the UFG microstructures in annealing treatments [24-26], relatively little attention has been given either to the development of texture in SPD processing or to the nature of the grain boundary misorientation distributions. However, both of these parameters play a significant role in determining the bulk properties of the materials. Some information has become available recently on the texture and grain boundary misorientation distributions after ECAP of pure Al and Al alloys [27-37], ECAP of pure Cu [38-40], ECAP and HPT of pure nickel [6, 41] and ECAP of pure Zr [42]. Although the results on pure Ni are fairly limited [41], the experimental data suggest that HPT produces a microstructure with a higher fraction of high-angle grain boundaries than ECAP. However, no systematic investigation has been conducted to date to examine the development of texture and the boundary misorientation statistics when processing by ECAP, by HPT and by a combination of these two processing procedures. Accordingly, the present investigation was initiated to provide this information.

Pure nickel was selected as a model material for use in this investigation and the experiments were conducted to determine the distribution of grain sizes, the texture and the characteristics of the grain boundary misorientation distributions using orientation imaging microscopy (OIM). Special attention was paid to an analysis of microtexture in order to detect specific crystallographic orientations existing in FCC materials under condition of pure shear.

## 2. EXPERIMENTAL MATERIAL AND PROCEDURES

High purity (99.99%) nickel was selected because experiments have shown that the stacking fault energy of pure Ni, which is intermediate between the stacking fault energies of pure Al and pure Cu, leads to a smaller grain size than in pure aluminum and a more homogeneous microstructure than in pure copper [43]. Prior to testing, the nickel was annealed for 6 hours at 973K to give an initial grain size of ~100 $\mu$m.

For processing by ECAP, cylindrical billets were machined having diameters of 16 mm and lengths of 130 mm and these billets were pressed at room temperature using a die having an internal angle, $\Phi$, of 90° between the two channels and an outer arc of curvature, $\Psi$, of 20° at the point of intersection of the channels. It can be shown from first principles that these values of $\Phi$ and $\Psi$ lead to an imposed strain of ~1 on each separate passage of the billet through the die [44]. All of the billets were pressed repetitively for a total of 8 passes under a pressure of ~800 MPa giving an equivalent strain of ~8, with the billets rotated by 90° in the same sense about the longitudinal axis between each separate pass in the processing procedure designated route $B_C$ [45]. After pressing, an electric-discharge facility was used to cut small disks from the centers of the cylinders, with the disks lying perpendicular to the longitudinal axes of the billets, and these disks were used for the subsequent measurements.

For HPT, samples were prepared in the form of disks having diameters of ~10 mm and thicknesses of ~0.3 mm and they were inserted into a torsion straining facility and subjected to a total of 5 complete revolutions at room temperature under an applied pressure of 6 GPa. Recognizing that it is difficult to precisely quantify the strain imposed in HPT [6], the strain is henceforth expressed solely in terms of the total numbers of turns or revolutions imposed on the sample.

In order to examine the potential for improving the microstructure and the subsequent properties through a combination of ECAP and HPT, an additional sample was prepared using one of the disks cut from a billet after ECAP and then subjecting this disk to HPT for 5 revolutions under an applied pressure of 6 GPa: this specimen is henceforth designated ECAP+HPT. Schematic illustrations of the processing procedures are given in Fig. 1.

The microtexture and the grain boundary misorientations were determined using OIM. The experimental data were collected using a Philips XL-30 FEG scanning electron microscope (SEM) with a TSL orientation imaging system. For a quantitative description of texture, it is necessary to define the laboratory coordinate system in order to perform a Bunge rotation [46] in Euler space. There is no unambiguous choice for the ECAP and HPT

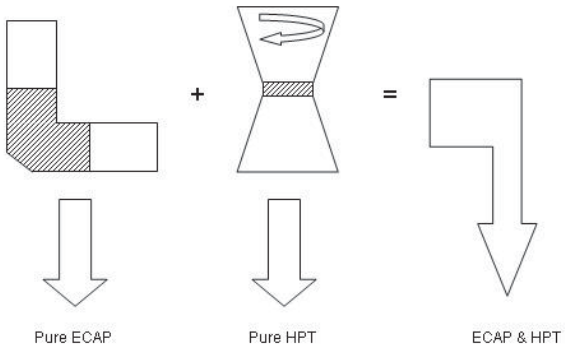


**Fig. 1.** Schematic representation of the processing procedures used in this investigation to produce UFG nickel.

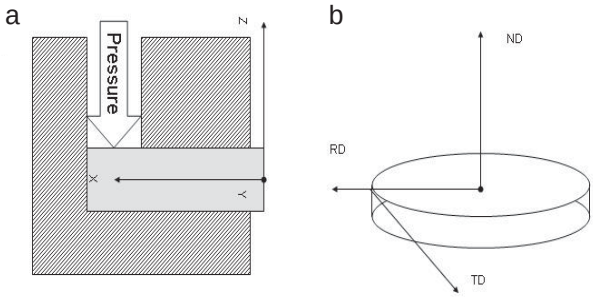


**Fig. 2.** Coordinate system adopted for ECAP (a) and HPT (b) samples.

processes and this contrasts with rolling where the normal direction (ND), rolling direction (RD) and transversal direction (RD) can be established. The same coordinate system is designated in the OIM system. For the ECAP process, the coordinate system suggested in earlier work [47] was used, as defined in Fig. 2a. There is some discussion in the literature concerning the equivalent description of the shear plane and shear direction. Recently [37], it was demonstrated that the shear plane in the ECAP sample can be equivalently described as the Z plane and the shear direction as parallel to the X axis in the coordinate system shown in Fig. 2a. A similar conclusion can be drawn from the paper by Segal [48], which describes the rotation of the plane for the principal shear stress in ECAP to the Z-plane orientation. For HPT, the natural choice for the coordinate system is shown in Fig. 2b where ND is perpendicular to the plane of the disc, RD is parallel to the radial direction and TD is parallel to the tangential direction.

## 3. EXPERIMENTAL RESULTS

The value of the mean grain size represents the key parameter in defining the nature of the UFG microstructure formed through SPD processing. In general, the mean grain size is usually determined from measurements taken using TEM but these measurements tend to be difficult because it is well established, after processing by both ECAP and HPT, that many of the boundaries in the as-processed material are diffuse in nature or represent transition zones between highly deformed grains. In addition, the boundary extinction contours are often very irregular due to the non-equilibrium character of the boundaries and the presence of many extrinsic dislocations. Nevertheless, preliminary observations by TEM gave mean grain sizes in the Ni samples of ~350 nm after ECAP, ~170 nm after HPT and ~140 nm after ECAP+HPT, respectively.

The lack of a homogeneous and clearly-defined array of equiaxed grains in many materials after SPD processing makes it difficult, if not impossible, to fully characterize the UFG microstructure in terms of the distribution of grain sizes. One possibility is to assume, *a priori*, that the distribution follows a log-normal function as in conventional ball-milling but it is not easy to confirm this assumption because the complex contrast in the TEM images makes it difficult to clearly differentiate between many of the individual grains. The problem of microstructural characterization can be significantly overcome through the use of OIM. Fig. 3 illustrates this problem by showing images taken by OIM (color coded picture based on inverse pole figure) for the samples prepared through all of the SPD processes: the stereographic triangle on the left shows the orientations of the individual grains recorded by OIM. It is apparent from inspection of the images that the microstructures in these conditions consist of a reasonably equiaxed array of grains with mean grain sizes in the range of ~0.3 μm, ~0.2 μm and ~0.1 μm for ECAP, HPT and ECAP+HPT samples, respectively.

Microtexture data, in the form of pole figures obtained from OIM measurements, are shown in Fig. 4 for samples prepared through ECAP, HPT and ECAP+HPT, respectively; also shown in Fig. 5 are 3D views of the corresponding orientation distribution functions (ODF) calculated using harmonic methods. Fig. 4 shows pole figures (001), (011) and

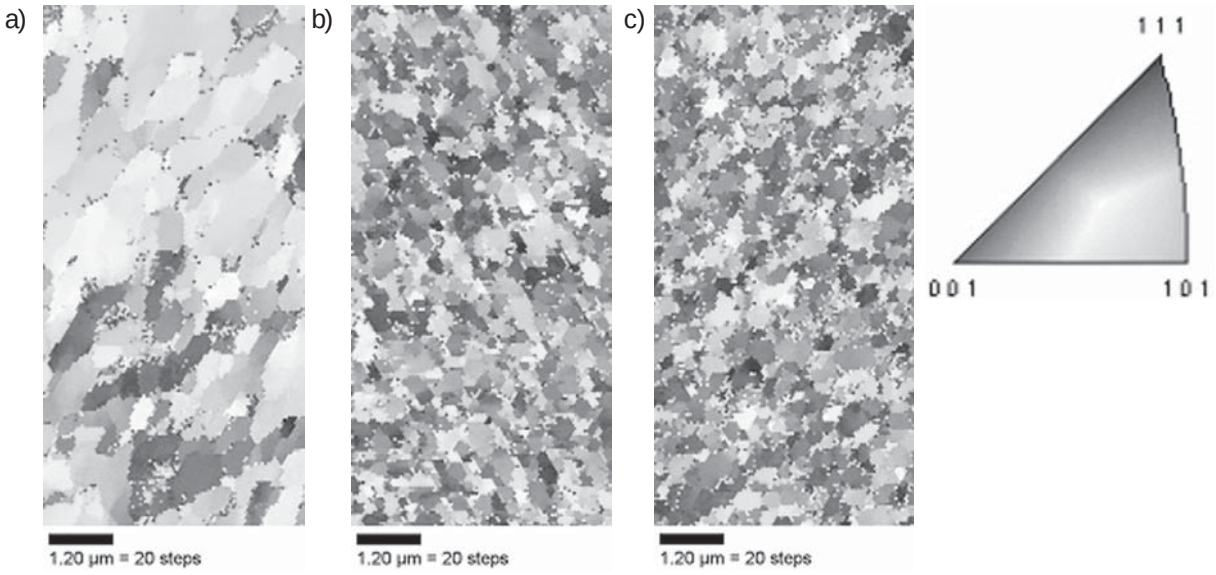


**Fig. 3.** Gray-scale coded microstructures of UFG nickel after ECAP (a), HPT (b) and ECAP+HPT (c) operations.

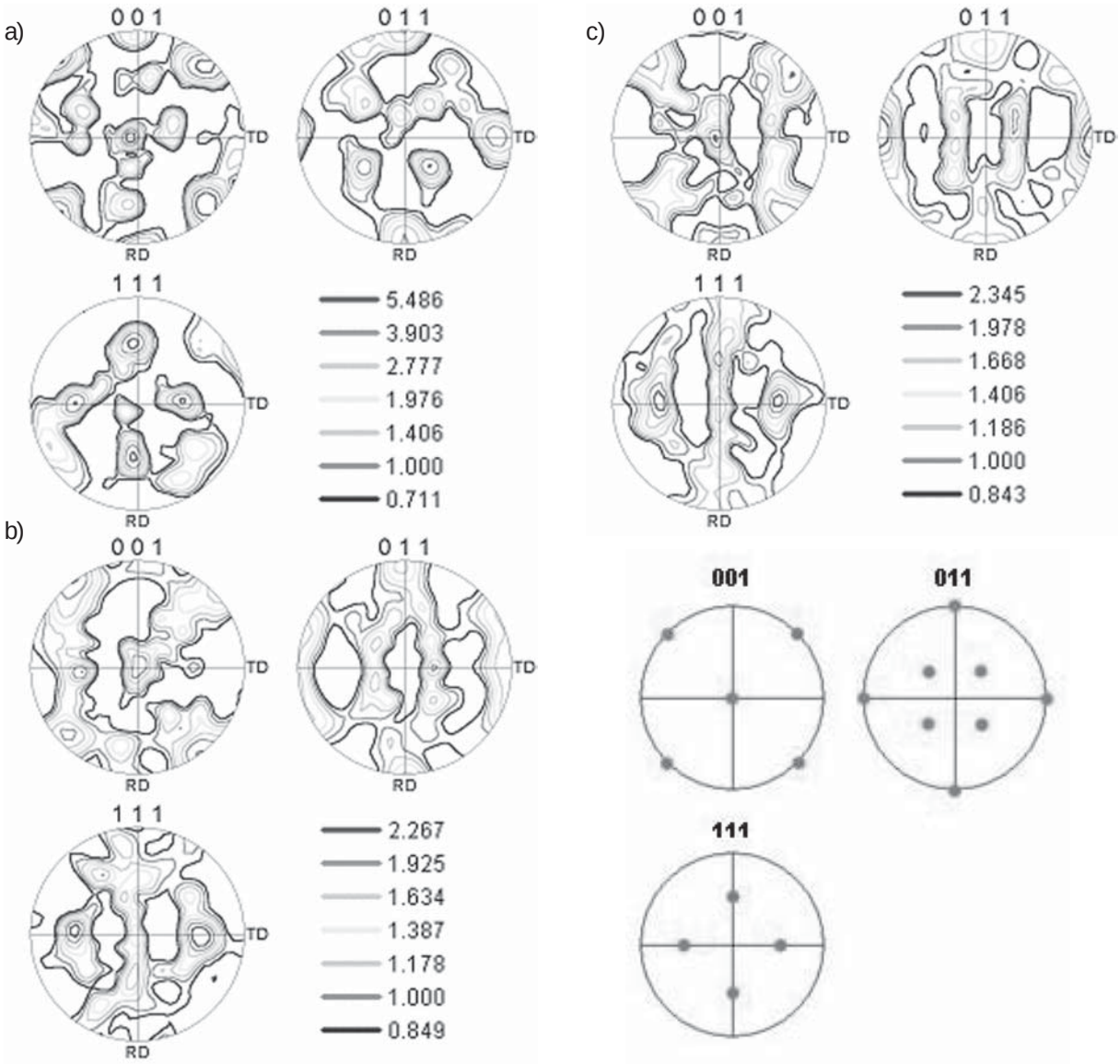


**Fig. 4.** Pole figures (001), (011), (111) for ECAP (a), HPT (b) and ECAP+HPT (c) nickel samples. Schematic view of the same pole figures for C-component of shear texture is shown.

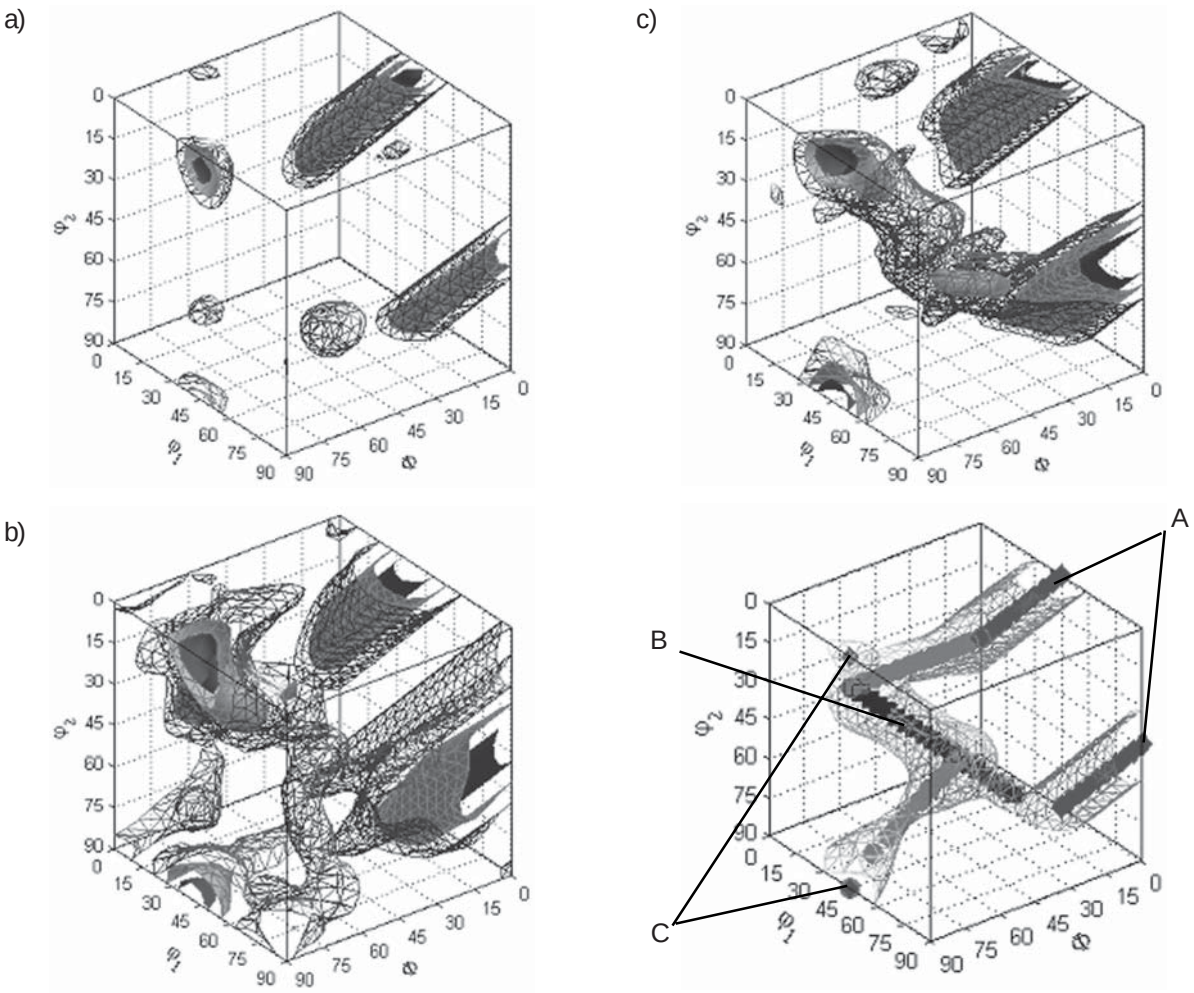


**Fig. 5.** 3D view of orientation distribution function for ECAP (a), HPT (b) and ECAP+HPT (c) nickel samples. Iso-surfaces of ¼, ½ and ¾ of maximum intensity are plotted. Schematic plot of A-fibers, B- fibers and C-components are presented in right down corner.

(111) types for UFG nickel obtained by ECAP (Fig. 4a), HPT (Fig.4b) and the combination of both (Fig. 4c). Following the work by Canova *et al.* [49], a detailed analysis of texture in pure aluminum after ECAP pressing was accomplished [50]. In particular, it was established that all three components of torsion texture revealed in [49], namely the C-component ({001}<110>), A- fiber ({111}<hkl>) and B-fiber ({hkl}<110>), are observed in ECAP pure aluminum. Similar features have been discovered in ECAP and HPT nickel samples. Major texture maxima correspond to the C- component schematically depicted on Fig. 4. The maximum of the C-component is stronger for ECAP nickel samples (~5.5 of random level) and there is a weak A-fiber present in the pole figures. The orientation distribution function plotted as 3D function in Euler angles ($\varphi_1$, $\Phi$, $\varphi_2$) is shown in Fig. 5. A schematic diagram of the A, B, C- components of pure shear texture is depicted on Fig. 5c, where the red squares correspond to C-component, green circles are $B_1$ and $B_2$ – fibers and blue line represents A-fiber.

The three dimensional ODF for ECAP, HPT and ECAP+HPT nickel samples are plotted in the form of iso-surfaces with ¼, ½, and ¾ of absolute maximum for corresponding orientation distributions. It is noted that the ECAP texture (Fig. 5a) consists mostly of C-component and it shows a minor maximum near the end of the A-fiber. The texture of the HPT and ECAP+HPT nickel samples possess more complex structures but nevertheless the C-component dominates.

The grain boundary misorientation distributions are shown in Fig. 6 for the three processing conditions of ECAP, HPT and ECAP+HPT in the form of the distribution of misorientation angle and the rel-

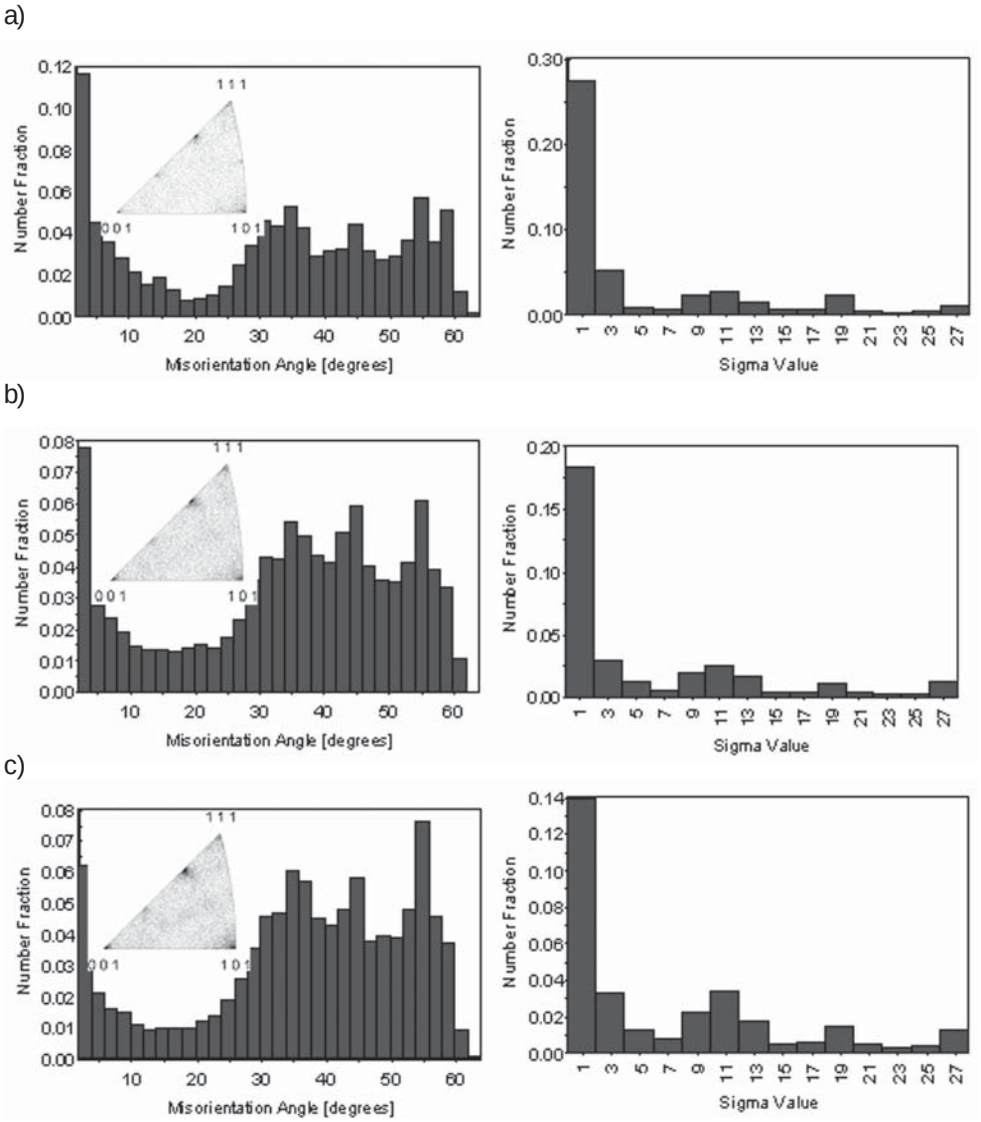


**Fig. 6.** Distribution of angle (left side) and axes (insets) misorientations and Sigma (right side) for ECAP (a), HPT (b) and ECAP+HPT (c) nickel.

evant axes are shown as insets. The corresponding fractions of low-angle (Σ1) boundaries having misorientations up to 15°, twin (Σ3) boundaries, other special (S5-30) boundaries and high-angle boundaries (HAB) having orientations >15° are depicted also as histogram. The misorientation angle in Fig. 6 denotes the measured disorientation angle between any two adjacent points in the OIM scan. Inspection of Fig. 6 shows the distributions are bimodal in character for all three processing conditions with peaks at both low (<15°) and high (>15°) angles. The peaks at angles <15° are not consistent with the theoretical prediction for a random distribution but the experiments show that the fraction of these low-angle boundaries is lower in HPT than in ECAP and there is an even greater reduction for the sample processed by ECAP+HPT. There is also evidence in all three distributions for the presence of two peaks at the higher angles, with these peaks lying in the vicinity of misorientation angles of ~35° and ~60°, respectively. A similar effect was reported in experiments on pure Al processed by ECAP [31] and the second peak corresponds to the twin misorientation.

It follows from Fig. 6 that the fraction of low-angle boundaries decreases from ~27% after ECAP to ~17% after HPT and ~14% after ECAP+HPT whereas a random distribution predicts a fraction of high-angle boundaries of ~90%.

## 4. DISCUSSION

Generally, relatively little attention has been given to the nature of the texture after SPD processing. However, there is a report of the evolution of texture in Cu processed by HPT where, with increasing strain in torsion, the intensity of the {200} peak decreased relative to the {111} peak giving an ultimate ratio after 5 turns of HPT of ~6.3 [51]. This result is not consistent with the present data for pure Ni where there is a strong axial texture of the {200} peak with a maximum of ~3 compared to a maximum for the {111} peak below 2.0 of random level. The texture in ECAP copper was measured and modeled very recently [52] and it was shown that it is similar to a shear texture that is characterized by distinct orientations of the C-component [49, 50]. After choosing an appropriate coordinate system and making a corresponding rotation of the OIM data, similar texture components were revealed in UFG nickel processed by ECAP, HPT and ECAP+HPT operations.

Inspection of Fig. 6 shows that the distributions of the misorientation angles for all UFG Ni specimens reveal a bimodal character with peaks within both the low and high angle ranges. In addition, the magnitude of the low-angle peak decreases in the order from ECAP to HPT to ECAP+HPT so that the reduction in the low-angle peak corresponds also to a reduction in the mean grain size. The presence of these low-angle peaks is a natural consequence of the very high strains, and thus the large numbers of dislocations, that are introduced into the materials during processing. Nevertheless, these low-angle peaks are not consistent with the theoretical predictions for a random distribution of misorientation angles. An important conclusion from the present investigation is that a combination of ECAP and HPT leads both to a finer homogeneous microstructure and to a higher fraction of high-angle boundaries with a general misorientation distribution that is significantly closer, as shown in Fig. 6, to the theoretical distribution.

According to the sigma value distribution (Fig. 6), ECAP processing leads also to a higher fraction of twin boundaries ($\Sigma 3$) by comparison with HPT. The fraction of twins after ECAP+HPT was also slightly higher than after HPT, thereby suggesting that the twin boundaries are reasonably stable when subjected to subsequent processing by HPT. Figure 6 shows also that all processing routes lead to a remarkably high fraction of special boundaries (S5-30) by comparison with the theoretical random distribution.

## 5. CONCLUDING REMARKS

1. Samples of pure nickel were processed by severe plastic deformation (SPD) using three distinct procedures: ECAP, HPT and ECAP+HPT. The results show the mean grain size is largest after ECAP, intermediate after HPT and the smallest grain size of ~140 nm was achieved after a combination of ECAP and HPT.
2. Texture measurements reveal a strong texture after ECAP and a weaker texture after HPT. There are common features for texture development in nickel samples during severe plastic deformation by ECAP and HPT (and also by their combination) and the texture reveals the main components (C-component, A- and B-fibers) typical for pure shear in materials subjected to torsion straining. A combination of ECAP and HPT leads to a similar texture as after pure HPT but with some deviations.
3. An analysis of grain boundary misorientation distributions reveals a higher fraction of low angle boundaries for ECAP nickel (about 27%) with the fraction decreasing for HPT (about 15-17%) and ECAP+HPT samples (below 15%).

## ACKNOWLEDGEMENTS

This work was supported in part by the National Science Foundation of the United States under Grant No. DMR-0243331 and INTAS-03513779. One of the authors (APZ) thanks the Spanish government (grant SAB 2000-0390) and the National Research Council of the National Academy of Science (USA) for financial support.

## REFERENCES

[1] R. Z. Valiev, I. V. Alexandrov, Y. T. Zhu and T. C. Lowe // *J. Mater. Res.* **17** (2002) 5.
[2] V. M. Segal, V. I. Reznikov, A. E. Drobyshevskiy and V. I. Kopylov // *Russ. Metall. (Metally)* **1** (1981) 99, in Russian.
[3] R. Z. Valiev, A. V. Korznikov and M. M. Mulyukov // *Mater. Sci. Eng. A* **168** (1993) 141.
[4] R. Z. Valiev, R. K. Islamgaliev and I. V. Alexandrov // *Prog. Mater. Sci.* **45** (2000) 103.
[5] N. A. Smirnova, V. I. Levit, V. I. Pilyugin, R. I. Kuznetsov, L. S. Davydova and V. A. Sazonova // *Fiz. Metal. Metalloved.* **61** (1986) 1170, in Russian.

[6] A. P. Zhilyaev, G. V. Nurislamova, B-K. Kim, M. D. Baró, J. A. Szpunar and T. G. Langdon // *Acta Mater.* **51** (2003) 753.
[7] Y. Saito, H. Utsunomiya, T. Sakai and R.G. Hong // *Scripta Mater.* **39** (1998) 1221.
[8] Y .Saito, H. Utsunomiya, N. Tsuji and T. Sakai // *Acta Mater.* **47** (1999) 579.
[9] N. Tsuji, Y. Saito, H. Utsunomiya and S. Tanigawa // *Scripta Mater.* **40** (1999) 795.
[10] R. S. Mishra, M. W. Mahoney, S. X. McFadden, N. A. Mara and A. K. Mukherjee // *Scripta Mater.* **42** (1999) 163.
[11] J-Q. Su, T. W. Nelson and C. J. Sterling // *J. Mater. Res.* **18** (2003) 1757.
[12] I. Charit and R.S. Mishra // *Mater. Sci. Eng. A* **359** (2003) 290.
[13] Y. S. Sato, Y. Kurihara, S. H. C. Park, H. Kokawa and N. Tsuji // *Scripta Mater.* **50** (2004) 57.
[14] A. P. Zhilyaev, G. V. Nurislamova, S. Surińach, M. D. Barň and T. G. Langdon // *Mater. Phys. Mech.* **5** (2002) 23.
[15] A.P. Zhilyaev, J. Gubicza, G. Nurislamova, Á. Révész, S. Surińach, M.D. Baró and T. Ungár // *Phys. Stat. Sol. (a)* **198** (2003) 263.
[16] A.P. Zhilyaev, J. Gubicza, S. Surińach, M.D. Baró and T.G. Langdon // M*ater. Sci. Forum* **426-432** (2003) 4507.
[17] S. X. McFadden, R. S. Mishra, R. Z. Valiev, A. P. Zhilyaev and A. K. Mukherjee // *Nature* **398** (1999) 684.
[18] V. M. Segal // *Mater. Sci. Eng. A* **197** (1995) 157.
[19] V. M. Segal // *Mater. Sci. Eng. A* **271** (1999) 322.
[20] M. Furukawa, Z. Horita, M. Nemoto and T.G. Langdon // *J. Mater. Sci.* **36** (2001) 2835.
[21] A.P. Zhilyaev, S. Lee, G.V. Nurislamova, R.Z. Valiev and T.G. Langdon // *Scripta Mater.* **44** (2001) 2753.
[22] Y. Iwahashi, Z. Horita, M. Nemoto and T.G. Langdon // *Acta Mater.* **45** (1997) 4733.
[23] Y. Iwahashi, Z. Horita, M. Nemoto and T.G. Langdon // *Acta Mater.* **46** (1998) 3317.
[24] J. Wang, Y. Iwahashi, Z. Horita, M. Furukawa, M. Nemoto, R.Z. Valiev and T.G. Langdon // *Acta Mater.* **44** (1996) 2973.
[25] H. Hasegawa, S. Komura, A. Utsunomiya, Z. Horita, M. Furukawa, M. Nemoto and T.G. Langdon // *Mater. Sci. Eng.* **A265** (1999) 188.
[26] A.P. Zhilyaev, G.V. Nurislamova, M.D. Baró, R.Z. Valiev and T.G. Langdon // *Metal. Mater. Trans.* **33A** (2002) 1865.
[27] A. Gholinia, P.B. Prangnell and M.V. Markushev // *Acta Mater.* **48** (2000) 1115.
[28] C.P. Chang, P.L. Sun and P.W. Kao // *Acta Mater.* **48** (2000) 3377.
[29] J.C. Huang, I.C. Hsiao, T.D. Wang and B.Y. Lou // *Scripta Mater.* **43** (2000) 213.
[30] J-Y. Chang, J-S. Yoon and G-H. Kim // *Scripta Mater.* **45** (2001) 347.
[31] S. D. Terhune, D. L. Swisher, K. Oh-ishi, Z. Horita, T.G. Langdon and T.R. McNelley // *Metall. Mater. Trans.* **33A** (2002) 2173.
[32] Z.C. Wang and P.B. Prangnell // *Mater. Sci. Eng. A* **328** (2002) 87.
[33] J.R. Bowen, O.V. Mishin, P.B. Prangnell and D. Juul Jensen // *Scripta Mater.* **47** (2002) 289.
[34] P.L. Sun, C.Y. Yu, P.W. Kao and C.P. Chang // *Scripta Mater.* **47** (2002) 377.
[35] Y.C. Chen, Y.Y. Huang, C.P. Chang and P.W. Kao // *Acta Mater.* **51** (2003) 2005.
[36] A. Goloborodko, O. Sitdikov, T. Sakai, R. Kaibyshev and H. Miura // *Mater. Trans.* **44** (2003) 766.
[37] A. Gholinia, P. Bate and P.B. Prangnell // *Acta Mater.* **50** (2002) 2121.
[38] O.V. Mishin, D. Juul Jensen and N. Hansen // *Mater. Sci. Eng. A* **342** (2003) 320.
[39] G. Wang, S.D. Wu, L. Zuo, C. Esling, Z.G. Wang and G.Y. Li // *Mater. Sci. Eng. A* **346** (2003) 83.
[40] L. S. Tóth, R. A. Massion, L. Germain, S. C. Baik and S. Suwas // *Acta Mater.* **52** (2004) 1885.
[41] A.P. Zhilyaev, B-K. Kim, G.V. Nurislamova, M.D. Baró, J.A. Szpunar and T.G. Langdon // *Scripta Mater.* **48** (2002) 575.
[42] W.S. Choi, H.S. Ryoo, S.K. Hwang, M.H. Kim, S.I. Kwun and S.W. Chae // *Metall. Mater. Trans.* **33A** (2002) 973.
[43] K. Neishi, Z. Horita and T.G. Langdon // *Mater. Sci. Eng. A* **325** (2002) 54.
[44] Y. Iwahashi, J. Wang, Z. Horita, M. Nemoto and T.G. Langdon // *Scripta Mater.* **35** (1996) 143.
[45] M. Furukawa, Y. Iwahashi, Z. Horita, M. Nemoto and T.G. Langdon // *Mater. Sci. Eng. A* **257** (1998) 328.
[46] H.-J. Bunge, *Texture Analysis in Materials Science – Mathematical Methods* (London, Butterworths, 1982).
[47] Y. Iwahashi, M. Furukawa, Z. Horita, M. Nemomoto and T. G. Langdon // *Metall. Trans.* **29A** (1998) 2245.

[48] V.M. Segal // *Mater. Sci. Eng. A* **345** (2003) 36.
[49] G.R. Canova, U.F. Kocks and J.J. Jonas // *Acta Metall.* **32** (1984) 211.
[50] D. Swisher, K. Oh-ishi, A. P. Zhilyaev and T. R. McNelley, (2004), to be published.
[51] H. Jiang, Y.T. Zhu, D.P. Butt, I.V. Alexandrov and T.C. Lowe // *Mater. Sci. Eng. A* **290** (2000) 128.
[52] L.S. Tóth, R.A. Maisson, L. Germain, S.C. Baik and S. Suwas // *Acta Mater.* **52** (2004) 1885.